Peer-reviewed version available at Minerals 2018, 8, 101; doi:10.3390/min8030101

Article

Dissolved silica effects on adsorption and co-precipitation of Sb(III) and Sb(V) with ferrihydrite

Shuang Zhou [1,*], Tsutomu Sato [2,*] and Tsubasa Otake [2]

[1] Graduate school of Engineering, Hokkaido University, Sapporo, Hokkaido, Japan 1; mzhou0327@gmail.com

[2] Faculty of Engineering, Hokkaido University, Sapporo, Hokkaido, Japan 2; tomsato@eng.hokudai.ac.jp

* Correspondence: mzhou0327@gmail.com; tomsato@eng.hokudai.ac.jp; Tel.: +81-11-706-6321

Abstract: Elevated antimony concentrations in aqueous environments from anthropogenic sources is becoming of global concern, here iron oxides are known to strongly adsorb aqueous antimony species with different oxidation states, but the effect of silica on the removal characteristics is not well understood despite being a common component in the environment. In this study, ferrihydrite was synthesized at various Si/Fe molar ratios to investigate its adsorption and co-precipitation behaviors with aqueous antimony anionic species, Sb(III) and Sb(V). The XRD analyses of the precipitates showed two broad diffraction features at approximately 35° and 62° 2θ, which are characteristic of 2-line ferrihydrite, no significant shifts in peak positions in the ferrihydrite regardless of the Si/Fe ratios. The infrared spectra showed a sharp band at ~990 cm^{-1}, corresponding to asymmetric stretching vibrations of Si-O-Fe bonds which increased in intensity with increasing Si/Fe molar ratios. Further, the surface charge on the precipitates became more negative with increasing Si/Fe molar ratios. The adsorption experiments indicated that Sb(V) was preferentially adsorbed at acidic conditions and decreased dramatically with increasing pH while the adsorption rate of Sb(III) ions was independent of pH, however, the presence of silica suppressed the adsorption of both Sb(III) and Sb(V) ions. The results showed that Sb(III) and Sb(V) ions were significantly inhibited by co-precipitation with ferrihydrite even in the presence of silica by isomorphous substitution in the ferrihydrite crystal structure.

Keywords: Antimony; Ferrihydrite; Silica; Adsorption; Co-precipitation

1. Introduction

Antimony (Sb) is widely used in industry as a catalyst in plastics, flame retardants, storage batteries, and ammunition [1][2][3]. It is the ninth most mined metal for industrial uses worldwide [4][5], and one result of this is elevated concentrations of Sb in many soils and waters, especially around mining and smelting areas [6][7][8][9][10][11][12]. There has been a growing concern over the adverse effect of Sb on human health due to its toxicity. Antimony has been increasingly identified as a toxic heavy metal with implications for it being a carcinogen [13]. This has caused antimony and its compounds to be listed as a leading pollutant by the United States Environmental Protection Agency [14] and the Council of the European Union [15].

Antimony may be present in a variety of oxidation states (-III ,0, III, V) because of its s^2p^3 outer orbital electron configuration, however it is mainly found in the two oxidation states (III and V) in environmental, biological, and geochemical environments [1][5]. The toxicity of Sb depends strongly on its oxidation state, and reduced Sb(III) species are ten times more poisonous than oxidized Sb(V), similar to the case of arsenic [16]. In spite of the widespread usage and the substantial toxicity, the geochemical behaviors of Sb in soil and aquatic systems are poorly understood [17][18].

Recent studies have shown that both Sb(III) and Sb(V) appear to adsorb strongly onto iron oxides [10][19][20][18], which thereby strongly influence the speciation, mobility, and final states of antimony in the environment. Antimony is preferentially associated with iron(III) oxyhydroxide in soils and sediments on the basis of direct evidence using extended X-ray absorption fine structure spectroscopy (EXAFS) [6][10][21]. This would suggest that adsorption and incorporation processes into the iron(III) (oxyhydr)oxide phases would be able to control the mobility of Sb in natural environments. Several experimental studies have investigated the Sb adsorption mechanism on iron(III) oxyhydroxides, focusing on Sb speciation at the solid-liquid (water) interface using EXAFS [10][22].

However, the surface structure of Sb(III) and Sb(V) biding with iron iron(III) oxyhydroxides is still unclear. A further important process, co-precipitation with iron(III) (oxyhydr)oxides, does not appear to have been reported. In natural systems, iron(III)(hydro)oxides are often identified in precipitates from the oxidation of Fe(II) in the presence of the relevant anions. Thus, the precipitation process may be as important as adsorption, as a sequestration process of Sb species by iron (III) (oxyhdr)oxides when groundwater with natural or added Fe comes in contact with air or oxygenated water.

Further, as Fe minerals are closely associated with silica, one of the most common ligands present in natural environments, pure ferrihydrite is not, strictly speaking, present in nature. Silica always associates with ferrihydrite in the structure or on the ferrihydrite surface. This could mean that silica may affect the crystallization behavior as well as the capacity of ferrihydrite to regulate hazardous element recycling. The effect of silica on arsenic adsorption has been reported for ferrihydrite [23], but no reports of the effect of silica on antimony adsorption or co-precipitation have been reported for other oxides.

Based on the above, the objectives of this study were to (1) compare the relative adsorption capabilities of Sb(III) and Sb(V) onto ferrihydrite. (2) to evaluate the effect of dissolved silica during the adsorption and co-precipitation of Sb(III) and Sb(V) on ferrihydrite, and also (3) to better understand the differences between the adsorption and co-precipitation processes of antimony.

2. Materials and Methods

2.1. Adsorption experiments

A stock solution of ferric iron (Fe(III), 0.05 mol/L), was prepared by dissolving reagent grade $Fe(NO_3)_3 \bullet 9H_2O$ (Kanto, 99%) in ultrapure water (18 M Ω•cm). Tetraethylorthosilicate (TEOS; Alfa Aesar, 98%) was then added to 500 mL of the Fe solution to achieve silica concentrations of 0 to 20 × 10^{-3} mol/L (i.e., Si/Fe = 0.4). These solutions containing both silica and Fe(III) were stirred for about 30 minutes

to dissolve the TEOS completely before pH adjustment. The initial pH of the solution was about 1.8, which was adjusted to about 7.0 ± 0.1 by titrating 1.0 M NaOH (Kanto, 97%). Addition of the NaOH hydrolyze the Fe(III) in the solution resulting in formation of a slurry of dark brown precipitates. The slurries were stirred for an additional 15 minutes to allow the pH to stabilize. The resulting 500 mL slurries were then equally divided into 50 mL polypropylene bottles and then washed in the bottles at least four times with deionized water to remove the salts and freeze-dried for at least 24 h. Samples with different silica concentrations were replicated to evaluate the reproducibility of the experimental results.

Stock solutions of Sb(V) were prepared by dissolving $KSb(OH)_6$ powder (Wako, 50%) into deionized water, and of Sb(III) by dissolving Sb_2O_3 powder (Wako, 98%) into 2 mol/L HCl (Kanto, 37%) solution. The adsorption experiments with either of Sb(III) and Sb(V) were conducted at a solid concentration of 0.5 g/L with a background ionic strength of 0.01 M NaCl. Triplicates of 40 mL suspensions with a fixed amount of solids (20 mg) and 100 μM solute concentrations were prepared in 50 mL plastic bottles. The experiments were conducted at a pH range of 3 – 12. The pH of the suspensions was adjusted using small volumes of 0.5 M HCl or 0.5 M NaOH during the experiments. Suspensions were agitated on a rotary shaker (110 rpm) for 24 h at 20.5 ℃ After the reaction, the suspensions were centrifuged and then filtered through a 0.2 μm cellulose membrane filter for the further analysis.

2.2. Co-precipitation experiments

The Sb(III) and Sb(V) co-precipitation experiments were conducted by hydrolysis of Silica and Fe(III) solution and either of Sb(III) and Sb(V) in deionized water, following the method of Waychunas et al. [24]. Coprecipitated samples were prepared by simultaneous addition either of 100 μM Sb(III) and Sb(V), 0.05 M Fe(III) solution, and the TEOS to yield the different Si/Fe ratios of the precipitate (Si/Fe = 0 to 0.4). In all cases, the Si/Fe ratios of the samples were determined assuming complete precipitation of all added Fe and Silica. The 500 mL mixed solutions were maintained at the experimental pH (7.0 ± 0.1) by the addition of 1.0

M NaOH. After precipitation and approximately 30 minutes of pH stabilization, the coprecipitates were washed at least four times with deionized water by centrifugation with a 50 mL plastic tube, then the suspension was filtered through a 0.2 μm cellulose membrane filter for the further analysis.

2.3. Analytical methods

Synthesized precipitates were analyzed by powder X-ray diffraction (XRD) using a Rigaku RINT2000 X-ray diffractometer operated at 40 kV and 40 mA, equipped with a Cu target and graphite monochromator, and diffraction profiles were collected from 10 to 70° 2θ.

The FTIR spectra were recorded from 400 to 4000 cm^{-1} by a JASCO FTIR-4100 spectrometer with a 1.0 cm^{-1} spectral resolution. The KBr used to prepare the sample was heated at 110 ℃for two hours prior to analysis to remove water. Pellets for analyzing were prepared by pulverizing the precipitates and mixing with KBr at a 1.5 mg precipitate to 250 mg KBr ratio.

The ζ-potential of the samples was measured using a Zetasizer Nano ZS90 (Malvern Zetasizer Nano series Nano-ZS90). Freeze-dried precipitates were resuspended in 10 mL deionized water to obtain the final mineral concentration of 100 mg/L. The auto-titration was initiated at pH values from 2 to 12 (in 0.5 pH increments) adjusting the pH with dilute HNO_3 and NaOH solutions.

Filtrates were analyzed for Sb(III) and Sb(V) as total antimony by Inductively Coupled Plasma Atomic Emission Spectroscopy (ICPE-9000, ICP-AES). The detection limit of this method was 0.1 μg/L. The pH of the solutions was measured with a pH meter (HORIBA, D-55) calibrated by using commercial pH 4.0, 7.0 and 10.0 buffer solutions. The amount of solute adsorbed was calculated using the difference between the initial and final dissolved solute concentrations.

3. Results and discussion

3.1. Characterization of initial adsorbents

The XRD analyses were conducted to determine the mineralogy of the dark brown precipitates. In all of the samples with the various initial ratios of Si/Fe, the XRD analyses of the dark brown precipitates, which were used as adsorbents in the following adsorption experiments, were characterized by two broad maxima centered at approximately 35° and 62° 2θ (Figure 1), consistent with the presence of 2-line ferrihydrite [25][26]. No significant shifts or changes in the width of the ferrihydrite 'peaks' in these precipitates were observed in the range of silica concentration studied.

To identify the chemical bonds in the initial adsorbents, FTIR analyses were conducted, and the infrared spectra of the initial adsorbents were generally consistent with published data on ferrihydrite [27]. There were significant changes with increasing silica concentrations in the precipitates. Specifically, a relatively sharp band at ~930 cm^{-1} corresponding to asymmetric stretching vibrations of Si-O-Fe bonds appeared and increased in intensity with increasing concentrations of silica (Figure 2), suggesting the presence of a small amount of polymeric Si [28].

To examine the surface charge properties of the initial adsorbents, the ζ-potential measurements at different pH were conducted. The ζ-Potential of the initial precipitates are shown as a function of pH in Figure 3. In general, the pH_{pzc} (point of zero charge) of ferrihydrite decreases with increasing silica content during the synthesis. For instance, the pH_{pzc} of ferrihydrite in the absence of silica was 8.2 and that of ferrihydrite at Si/Fe = 0.4 was 4.8, suggesting that the surface of the initial precipitates was more negatively charged after the Silica loading.

The XRD results indicate that the Si/Fe of the precipitating solution does not influence the mineralogy of the initial precipitates. Rapid hydrolysis of the Fe(III) in solution due to the addition of NaOH resulted in the co-precipitation of silica and Fe into poorly ordered ferrihydrite. The FTIR data show that silica became closely associated with the ferrihydrite via the formation of Si-O-Fe groups, but it is not

clear if silica is incorporated into the structure of ferrihydrite. Pokrovski [29] has demonstrated that aqueous silica may form stable iron silicate aqueous complexes with polymeric ferric oxy-hydroxide species. However, recent studies have shown that silica could also occur on the surface [30][31][32]. Detailed IR studies of adsorbed silica on ferrihydrite surfaces show the formation of bidentate surface complexes composed of monomeric silicate species at low silica ratios, similar to the concentrations used in this study [33]. Formation of these silica surface complexes results in a net release of protons that decreases the positive charge on the precipitate surface [34]. This is consistent with the changes in the ζ-potential observed with increasing Si/Fe ratios (Figure 3). At high Si ratios, the surface can be expected to become more negative as the silica polymerizes and creates more acidic surface complexes [28].

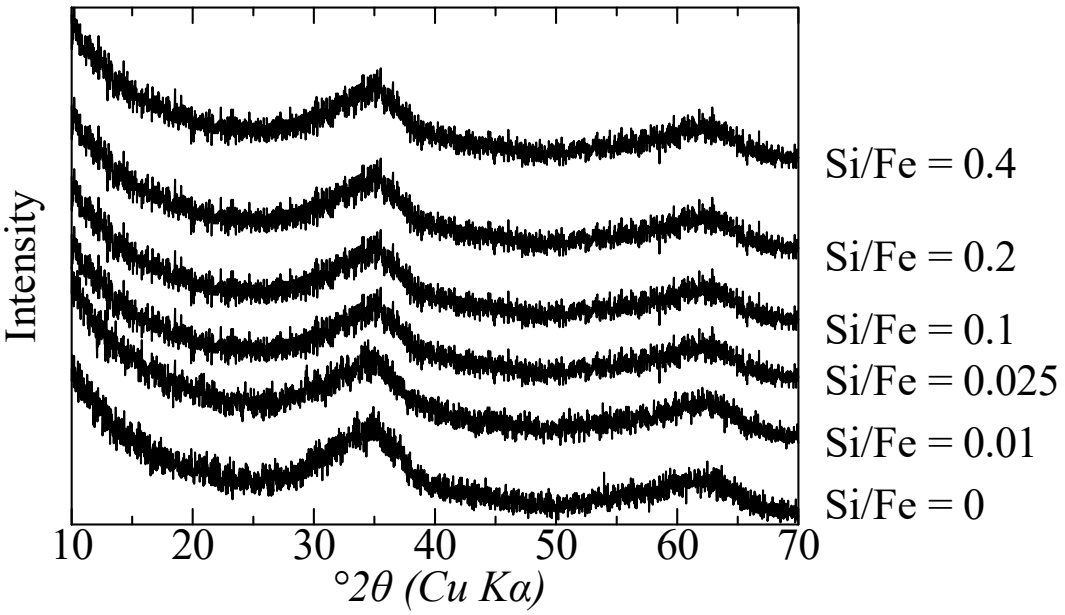

Figure 1. XRD spectra of the initial synthetic precipitates with different Si/Fe ratios.

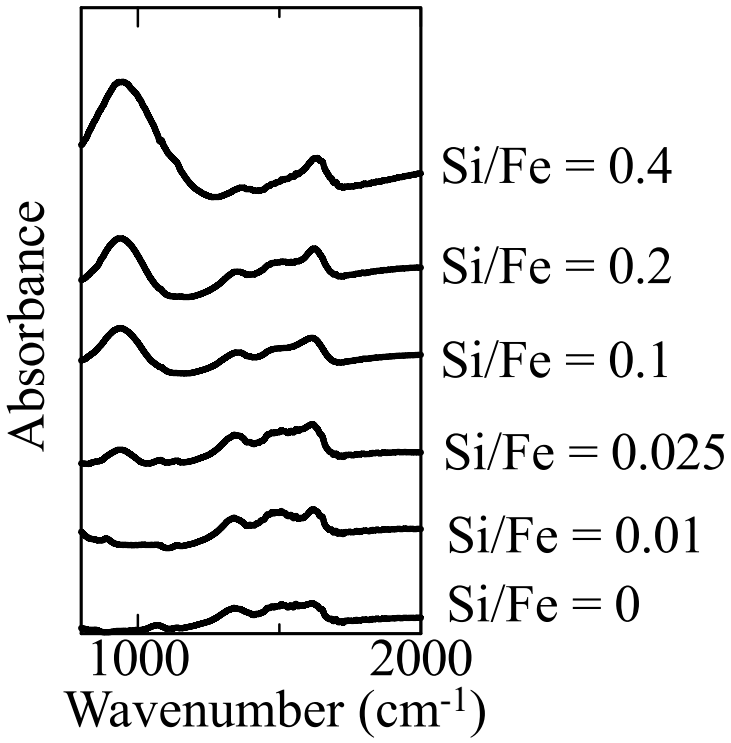

185

186 **Figure 2.** FTIR spectra of the initial synthetic precipitates with different Si/Fe ratios.

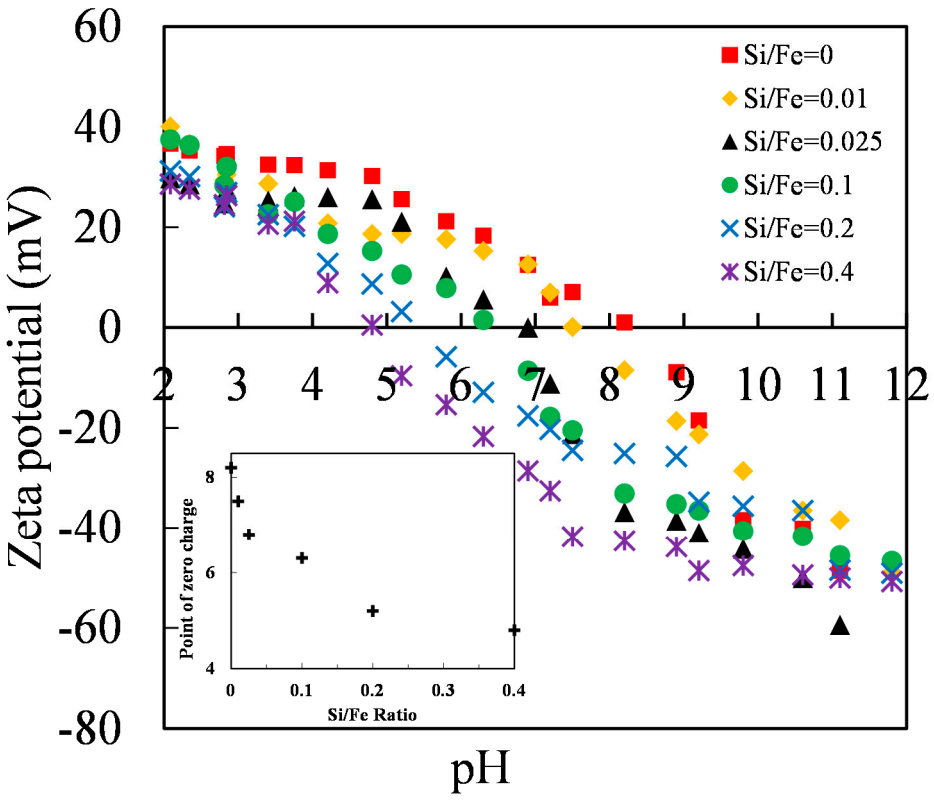

187

188 **Figure 3.** Changes in the ζ-potential of ferrihydrite at different Si/Fe ratios as a function of pH in 0.01 M NaCl.

3.2. Adsorption of Sb(III) and Sb(V) on ferrihydrite

3.2.1. Sb(III) and Sb(V) adsorption in the absence of silica

The adsorbed ratios of Sb(III) and Sb(V) ions onto ferrihydrite in 0.01 M NaCl solutions is shown as a function of pH in Figure 4. The adsorption rate of Sb(V) was over 90 % between pH 3 and 6. With increasing pH, from 6 to 12, the adsorption rate of Sb(V) rapidly decreased from 90% to 10%. A strong pH dependence on Sb(V) adsorption has been reported when goethite and ferrihydrite were used as adsorbents ([22][35]). The effect of pH on Sb(III) adsorption however was much weaker, showing a constant adsorbed fraction ~95% over the whole of the pH range investigated here, from 3 to 12. This is in good agreement with earlier studies [36][22]. The difference in adsorption efficiency of Sb(III) and Sb(V) ions may mainly be due to differences in the electrostatic interactions between the sorbent surface and antimony oxyanions present in the solutions. The $Sb(OH)_6^-$ is the dominant Sb(V) species over the wide pH range, here (3 – 10) [1]. The surface charge of ferrihydrite is positive below pH ~8.2, pH_{pzc}, and electrostatic attraction between the $Sb(OH)_6^-$ and the surface of ferrihydrite can be expected to be stronger under acidic conditions since $Sb(OH)_6^-$ is negatively charged at the conditions here, leading to the electrostatic forces playing an important role in the Sb(V) adsorption. For Sb(III), a trihydroxy neutral species, $Sb(OH)_3^0$, is the dominant species over a wide pH range (2 – 11) [1], and only minor or no electrostatic effects may be expected for the Sb(III) adsorption.

A specific interaction (so-called surface complexation) may also play an important role between the adsorbate and adsorbent in addition to the electrostatic effect. To evaluate the effects of surface complexation reactions of Sb(III) and Sb(V) on ferrihydrite, ζ-potential measurements were carried out after the adsorption experiments at different pH values. A ζ-Potential analysis is able to indirectly discriminate between inner- and outer-sphere surface complexes on mineral solid surfaces, as the formation of charged inner-sphere surface complexes changes the ζ-potential values and the pH_{pzc} (point of zero charge) because the ion adsorption occurs inside the shear plane [37]. The ζ-Potential over a wide pH range, from 3 to 12, and a significant pH_{pzc} shift was observed (Figure 5) for both Sb(III) and Sb(V) adsorption on ferrihydrite. The pH_{pzc} of the ferrihydrite after adsorbing Sb(V) is 7.1, which is higher than the 6.1 of Sb(III) (Figure 5). The shifts in pH_{pzc} are likely due to negative charges generated by inner-sphere complexation of Sb ions on the surface of ferrihydrite,

and the results of the ζ-potential measurements suggest that Sb(V) ions are adsorbed on the ferrihydrite surface but not as strongly as Sb(III) ions. The strong pH dependence on Sb(V) adsorption (Figure 4) suggests that electrostatic interactions play an important role for Sb(V) ions, and the strong pH dependence and shifts in pH_{pzc}. Together, these results imply that both outer- and inner-sphere complexes rather than only inner-sphere complexes contribute to the adsorption of Sb(V) ions on the ferrihydrite. Wang [38] has reported that a combination of outer and inner-sphere complexes for Sb(V) adsorption on iron modified aerobic granules, which is consistent with the results for Sb(V) adsorption here.

At the same time, the steep decrease in the pH_{pzc} by Sb(III) adsorption on ferrihydrite suggests that the uncharged Sb(III) is bound strongly to the surface of ferrihydrite by inner-sphere complexation, and the surface complexation between Sb(III) and Fe species is likely the dominating mechanism for Sb(III) adsorption, which would also be consistent with the pH independence of Sb(III) adsorption (Figure 4). An inner-sphere formation for bidentate mononuclear edge-sharing between Sb(III) and HFO was reported by using extended X-ray absorption fine structure (EXAFS) [22]. However, further spectroscopic evidence is necessary to understand the adsorption mechanism of Sb(III) and Sb(V) on the mineral surface in more detail.

All of the above results suggest that Sb(III) showed a higher adsorption efficiency toward ferrihydrite than Sb(V) in the pH range 6 – 12. Previous studies also reported more effective removal of Sb(III) than Sb(V) by ferric chloride over a broad pH range and under a variety of competing ions such as phosphate and humic acid [39].The comparison in mobility between the two Sb species appears to be different from that for the As(III) and As(V) species despite Sb and As belonging to the same group of the periodic table. Here the relatively stronger adsorption of Sb(III) compared to As(III) could be attributed to antimonite as a stronger Lewis base than arsenite [40], having a higher pKa value ($pKa1(H_3AsO_3)$ = 9.22; $pKa(Sb(OH)_3)$ = 11.9). The ferrihydrite is frequently amphoteric, and if considering the surface sites of ferrihydrite as Lewis acids, this would explain the stronger binding of Sb(III).

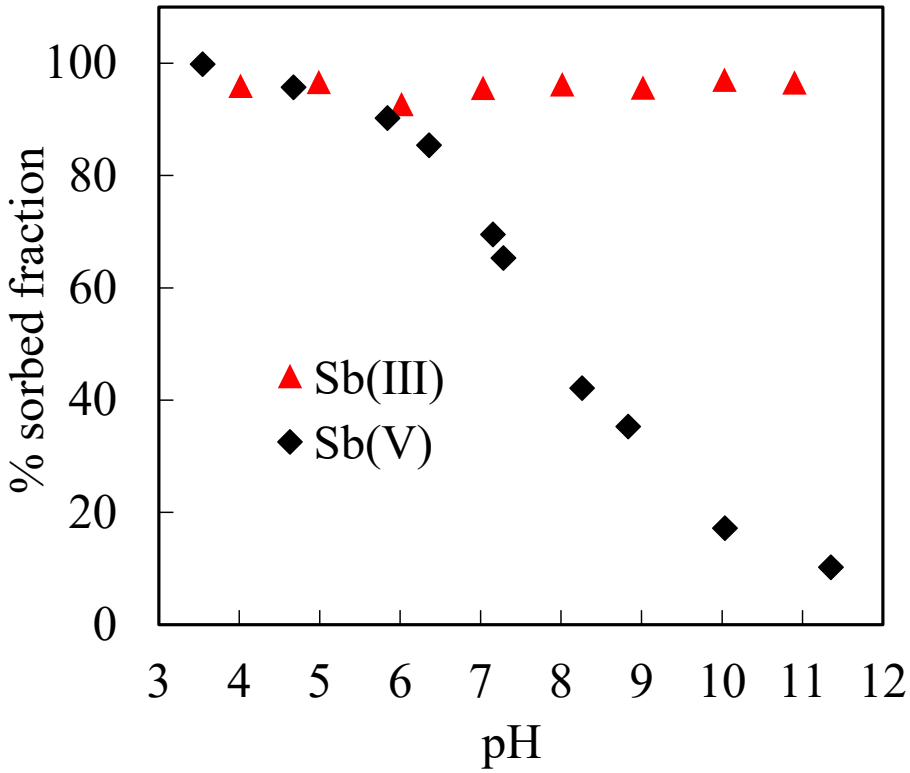

Figure 4. Adsorption of Sb(III/V) onto ferrihydrite as a function of the pH in 0.01 M NaCl solutions. The initial Sb(III/V) concentration were 100 μM for each sample. The concentrations of suspended solids were 0.5 g/L.

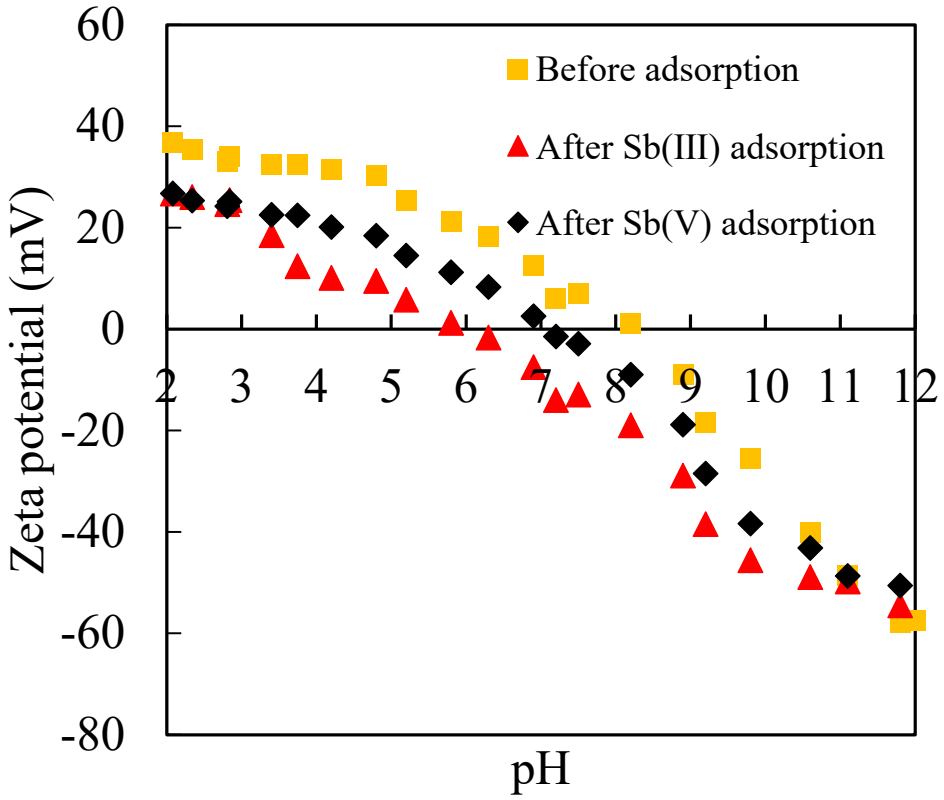

Figure 5. Changes in the ζ-potential of ferrihydrite after adsorbing Sb(III/V) as a function of pH in 0.01 M NaCl. The initial Sb(III/V) concentrations were 100 μM for all samples. The concentrations of suspended solids were 0.5 g/L.

3.2.2. Sb(III) and Sb(V) adsorption in the presence of silica

The effect of silica on the adsorption of Sb was investigated by varying the Si/Fe ratio of the precipitates at pH 7. The results demonstrated that both Sb(III) and Sb(V) are significantly affected by the presence of silica, with the adsorbed fraction decreasing with increasing Si/Fe ratios (Figure 6). Both Sb(III) and Sb(V) adsorption were suppressed in the presence of silica. The adsorbed fractions of Sb(III) and Sb(V) ions decreased from >96% at Si/Fe = 0 to 60% at Si/Fe = 0.4 and from >75% at Si/Fe = 0 to 30% at Si/Fe = 0.4, respectively. This shows that Sb(V) was affected more significantly by silica than Sb(III). The drop in Sb(V) adsorption efficiency is likely a result of decreased electrostatic interactions between Sb(V) ions and the surface of ferrihydrite by the decreased surface charge of ferrihydrite due to the presence of silica on the ferrihydrite surface (Figure 3), as discussed in the previous section, 3.1. Swedlund [23] also suggested that the decreasing surface charge of ferrihydrite by increasing silica concentrations could be an important factor in inhibiting As adsorption. Besides

the effect of silica to decrease the surface charge, silica may also suppress adsorption of Sb by occupying surface sites by the inner sphere complexation. No apparent pH_{pzc} shift was observed after adsorption of either Sb(III) or Sb(V) on ferrihydrite synthesized at Si/Fe = 0.2 (Figure 7). This suggests that Sb(III) or Sb(V) ions could not make enough inner-sphere complexes with surface ≡FeOH groups on ferrihydrite to change the ζ-potential because potential surface sites were already occupied by silica. This effect would be more important with Sb(III) ions since inner-sphere complexation is the dominating adsorption mechanism for Sb(III) ion onto ferrihydrite. Jordan [41] also showed that silicic acid could inhibit the retention of oxyanions of selenium onto hematite surfaces by competition with the surface sites of hematite. This suggests that a competition for surface sites on ferrihydrite could be a possible mechanism for inhibition of Sb adsorption.

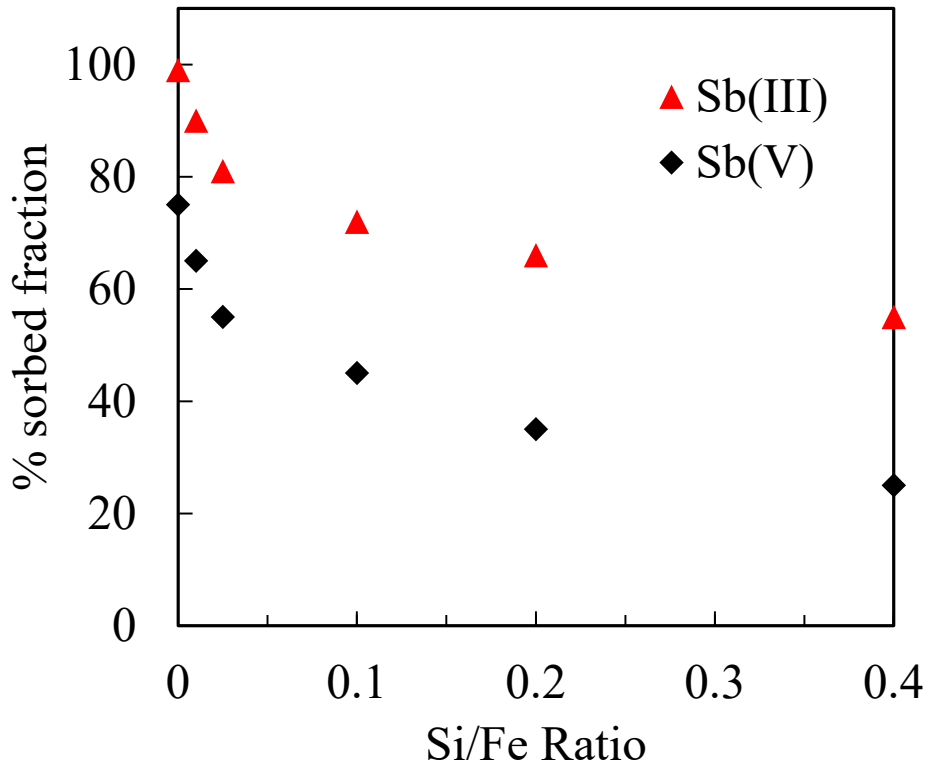

Figure 6. Adsorption of Sb(V) onto ferrihydrite with different Si/Fe ratios in 0.01 M NaCl solution at pH 7. The initial Sb(III) concentration were 100 μM. The concentrations of suspended solids were 0.5 g/L.

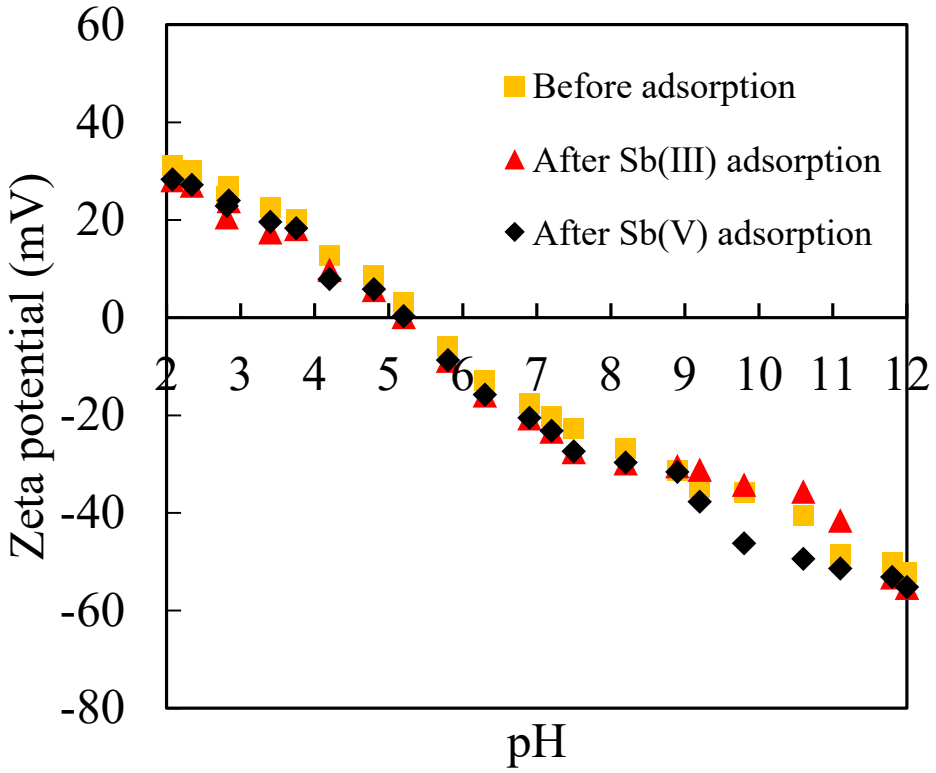

277

278 **Figure 7.** Changes in the ζ-potential of Si-ferrihydrite(Si/Fe=0.2) after adsorbing Sb(III/V) as a function of pH in
279 0.01 M NaCl. The initial Sb(III/V) concentrations were 100 μM for all samples. The concentrations of
280 suspended solids were 0.5 g/L.

281 *3.3. Sb(III) and Sb(V) co-precipitation process with different Si/Fe ratios*

282 The co-precipitation efficiencies were calculated using the difference between the initial and
283 final dissolved solute concentrations. Figure 8 shows the co-precipitation rates of Sb(III) and Sb(V)
284 ions with different Si/Fe ratios of ferrihydrite at pH 7. The co-precipitation efficiencies were ~100%
285 for both Sb(III) and Sb(V) in the absence of silica (Si/Fe = 0). No effect of silica was observed even at
286 the highest Si/Fe ratio in this study (Si/Fe = 0.4). Here the Sb(V) octahedra may replace Fe octahedrals
287 due to their structural compatibility. By using EXAFS spectroscopy analysis, Scheinost [6] has
288 reported that the Sb(V) can form both edge-sharing and corner-sharing inner-sphere complexes to Fe
289 oxides in shooting range soils, which would be consistent with our findings.

290 In the case of Sb(III) co-precipitation, with octahedral or tetrahedral structures absent in
291 Sb(III), the Sb(III) ions could alternatively be surrounded by Fe hydroxides, which would increase
292 the co-precipitation efficiency. While more specific evidence is necessary to explore the

co-precipitation mechanism of Sb(III) with ferrihydrite since no previous study has discussed issues related to this.

The absence of any effect of silica on the Sb(III) and Sb(V) co-precipitation process may be because of isomorphous substitution during the simultaneous addition of silica and Sb to the co-precipitation system. Specifically, the Si occupies a tetrahedral environment, being surrounded by 4 oxygen centers. These tetrahedral structures may share corners with two adjacent edge-sharing Fe octahedrals. This has been proposed by Pokrovski [42] on the basis of Fe K-edge extended X-ray absorption fine structure studies of Fe(III) hydrolyzed in the presence of silica. In addition, the tetrahedral Si could also coordinate with Fe tetrahedral structures since the ferrihydrite also has a tetrahedral structure as has been demonstrated by a previous study [43]. If so the silica may incorporate into the ferrihydrite structure during the co-precipitation process, which makes it more likely to have only a minor effect on the Sb retention.

Significant differences were observed in the results of the adsorption and co-precipitation experiments. The co-precipitation of Sb(III) and Sb(V) with ferrihydrite is much more effective than that of the adsorption with or without Sb(III) and Sb(V) in aqueous environments. Intuitively, the adsorption process in our experiments was solely due to adsorption onto the ferrihydrite surface, a surface complexation reaction. The co-precipitation process which in principle could include the formation of phases containing Sb(III) and Sb(V) in the structure as well as adsorbing Sb(III) and Sb(V) as an impurity onto the surface of ferrihydrite. This implies that Fe minerals can act as effective scavengers of Sb in natural environments where ferrihydrite is formed.

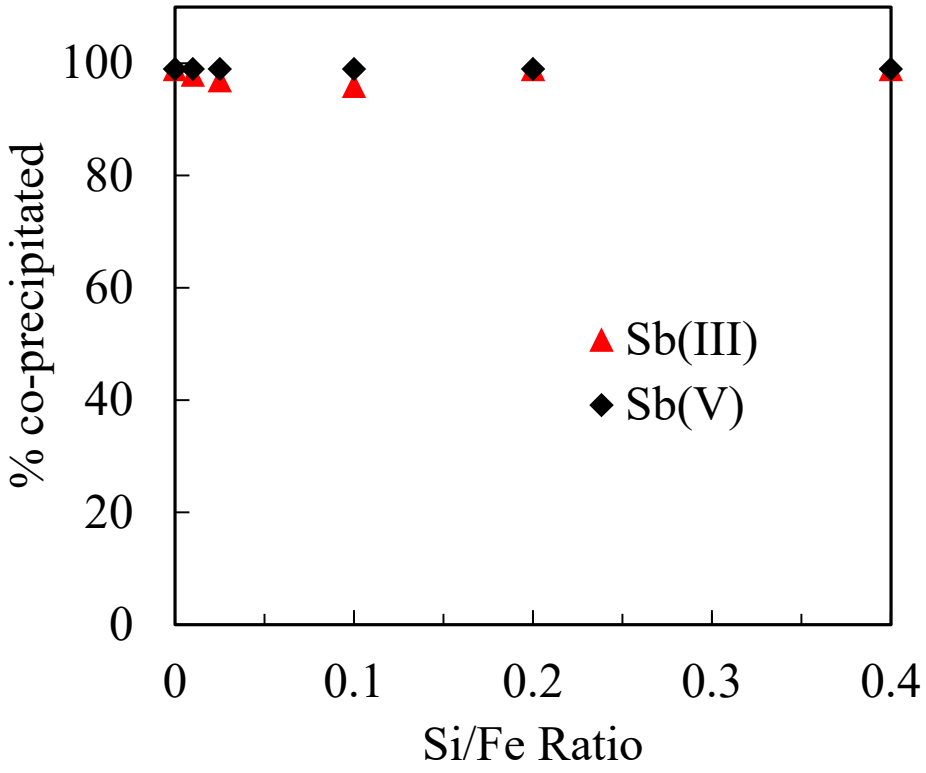

313

314 **Figure 8.** Co-precipitation of Sb(III/V) with different Si/Fe ratios of ferrihydrite at pH 7. The initial Sb(III/V)

315 concentrations were 100 μM for all samples.

316 **4. Conclusions and implications**

317 This study examined dissolved silica effects on the adsorption and
318 co-precipitation of Sb(III) and Sb(V) with ferrihydrite. The Sb(V) adsorption onto
319 ferrihydrite increased in more acidic conditions. Overall, Sb(III) adsorption was
320 constant over a broad pH range. The adsorption of Sb(III) and Sb(V) appeared to be
321 significantly affected by the presence of silica, while co-precipitation of Sb(III) and
322 Sb(V) with ferrihydrite was not inhibited by silica. Further, the co-precipitation
323 process takes place with higher efficiency than that of the adsorption.

324 Our findings on the behavior of Sb(III) and Sb(V) adsorption and
325 co-precipitation with ferrihydrite and Si-ferrihydrite have important implications
326 for determining the role of ferrihydrite in controlling the final state of Sb in the
327 environments it is released in. Although ferrihydrite is an excellent substance for
328 capturing Sb, its use as a medium in a natural Si-rich system should be considered

329 with caution because it will tend towards inhibition of Sb capture induced by the
330 Si-rich environment. However, this may be different in the case of co-precipitation
331 processes. In the present study, we found that both Si and Sb(III) and Sb(V) can be
332 incorporated into ferrihydrite and that these three are structurally compatible with
333 ferrihydrite. The co-precipitation process of Sb(III) and Sb(V) would not be greatly
334 influenced by the Si factor. Thus, Sb(III) and Sb(V) co-precipitation with ferrihydrite
335 would be more efficient than Sb(III) and Sb(V) adsorption by ferrihydrite. This
336 finding will be important when making predictions of the final state of Sb
337 associated with ferrihydrite in natural Si-rich system.

338 **Acknowledgments**

339 Shuang Zhou thanks the China Scholarship Council (CSC) and Hokkaido
340 University for financial support.

341 **Author Contributions**

342 Shuang Zhou and Tsutomu Sato conceived and designed the experiments;
343 Shuang Zhou performed the experiments; Shuang Zhou analyzed the data; Shuang
344 Zhou wrote the paper; Tsutomu Sato and Tsubasa Otake performed revisions;
345 Tsutomu Sato and Tsubasa Otake gave final approval of the paper to be published.

346 **Conflicts of Interest**

347 The authors have no conflict of interest to declare.

348 ## References

349 1. Filella, M.; Belzile, N.; Chen, Y. W. Antimony in the environment: A review focused on
350 natural waters I. Occurence. *Earth-Science Rev.* **2002**, *57*, 125–176,
351 doi:10.1016/S0012-8252(01)00070-8.

352 2. Carlin Jr, J. F. Antimony. *US Geol. Surv. Miner. Commod. Summ.* **2000**, 295–306.

353 3. Herbst, K. A.; Rose, G.; Hanusch, K.; Schumann, H.; Wolf, H. U. Antimony and antimony
354 compounds. *Ullmann's Encycl. Ind. Chem.* **1985**, *3*, 55–76.

355 4. Krachler, M.; Emons, H.; Zheng, J. Speciation of antimony for the 21st century: Promises and
356 pitfalls. *TrAC - Trends Anal. Chem.* **2001**, *20*, 79–90, doi:10.1016/S0165-9936(00)00065-0.

357 5. Filella, M.; Belzile, N.; Chen, Y. W. Antimony in the environment: A review focused on

natural waters II. Relevant solution chemistry. *Earth-Science Rev.* **2002**, *59*, 265–285, doi:10.1016/S0012-8252(02)00089-2.

6. Scheinost, A. C.; Rossberg, A.; Vantelon, D.; Xifra, I.; Kretzschmar, R.; Leuz, A. K.; Funke, H.; Johnson, C. A. Quantitative antimony speciation in shooting-range soils by EXAFS spectroscopy. *Geochim. Cosmochim. Acta* **2006**, *70*, 3299–3312, doi:10.1016/j.gca.2006.03.020.

7. He, M. Distribution and phytoavailability of antimony at an antimony mining and smelting area, Hunan, China. *Environ. Geochem. Health* **2007**, *29*, 209–219, doi:10.1007/s10653-006-9066-9.

8. Wang, X.; He, M.; Xi, J.; Lu, X. Antimony distribution and mobility in rivers around the world's largest antimony mine of Xikuangshan, Hunan Province, China. *Microchem. J.* **2011**, *97*, 4–11, doi:10.1016/j.microc.2010.05.011.

9. Westerhoff, P.; Prapaipong, P.; Shock, E.; Hillaireau, A. Antimony leaching from polyethylene terephthalate (PET) plastic used for bottled drinking water. *Water Res.* **2008**, *42*, 551–556, doi:10.1016/j.watres.2007.07.048.

10. Mitsunobu, S.; Harada, T.; Takahashi, Y. Comparison of antimony behavior with that of arsenic under various soil redox conditions. *Environ. Sci. Technol.* **2006**, *40*, 7270–7276, doi:10.1021/es060694x.

11. Lichti, K. a.; Ko, M.; Wallis, L. Galvanic corrosion study of carbon steel to arsenic and antimony couples. *Geothermics* **2015**, *58*, 15–21, doi:10.1016/j.geothermics.2015.07.006.

12. Okkenhaug, G.; Zhu, Y. G.; He, J.; Li, X.; Luo, L.; Mulder, J. Antimony (Sb) and Arsenic (As) in Sb mining impacted paddy soil from Xikuangshan, China: Differences in mechanisms controlling soil sequestration and uptake in Rice. *Environ. Sci. Technol.* **2012**, *46*, 3155–3162, doi:10.1021/es2022472.

13. Gebel, T. Aresnic and antimony: Comparative approach on mechanistic toxicology. *Chem. Biol. Interact.* 1997, *107*, 131–144.

14. USEPA Water Related Fate of the 129 Priority Pollutants. *USEPA, Washington, DC* **1979**, *1*, DOC. 745-R-00-007.

15. CEC Council Directive 76/substances discharged into Aquatic Environment of the Community. *Off. J. L.* **1976**, *129*, 23–29.

16. Oorts, K.; Smolders, E.; Degryse, F.; Buekers, J.; Gascó, G.; Cornelis, G.; Mertens, J. Solubility and toxicity of antimony trioxide (Sb2O3) in soil. *Environ. Sci. Technol.* **2008**, *42*, 4378–4383, doi:10.1021/es703061t.

17. Krupka, K. M.; Serne, R. J. *Geochemical Factors Affecting the Behavior of Antimony, Cobalt, Europium , Technetium, and Uranium in Vadose Sediments*; 2002;

18. Mitsunobu, S.; Takahashi, Y.; Terada, Y.; Sakata, M. Antimony(V) incorporation into synthetic ferrihydrite, goethite, and natural iron oxyhydroxides. *Environ. Sci. Technol.* **2010**, *44*, 3712–3718, doi:10.1021/es903901e.

19. Leuz, A.-K.; Mönch, H.; Johnson, C. A. Sorption of Sb (III) and Sb (V) to goethite: influence on Sb (III) oxidation and mobilization. *Environ. Sci. Technol.* **2006**, *40*, 7277–7282.

20. Okkenhaug, G.; Amstätter, K.; Lassen Bue, H.; Cornelissen, G.; Breedveld, G. D.; Henriksen, T.; Mulder, J. Antimony (Sb) contaminated shooting range soil: Sb mobility and immobilization by soil amendments. *Environ. Sci. Technol.* **2013**, *47*, 6431–6439, doi:10.1021/es302448k.

21. Ackermann, S.; Gieré, R.; Newville, M.; Majzlan, J. Antimony sinks in the weathering crust of bullets from Swiss shooting ranges. *Sci. Total Environ.* **2009**, *407*, 1669–1682, doi:10.1016/j.scitotenv.2008.10.059.

22. Guo, X.; Wu, Z.; He, M.; Meng, X.; Jin, X.; Qiu, N.; Zhang, J. Adsorption of antimony onto iron oxyhydroxides: Adsorption behavior and surface structure. *J. Hazard. Mater.* **2014**, *276*, 339–345, doi:10.1016/j.jhazmat.2014.05.025.

23. Swedlund, P. J.; Webster, J. G. Adsorption and polymerisation of silicic acid on ferrihydrite, and its effect on arsenic adsorption. *Water Res.* **1999**, *33*, 3413–3422, doi:10.1016/S0043-1354(99)00055-X.

24. Waychunas, G. . A.; Rea, B. . A.; Fuller, C. . C.; Davis, J. . A. Surface chemistry of ferrihydrite: Part 1.EXAFS studies ongeometrie of coprecipitated and adsorbed arsenate. *Geochim. Cosmochim. Acta* **1993**, *57*, 2251–2269, doi:10.1016/0016-7037(93)90567-G.

25. Russell, J. D. Infrared spectroscopy of ferrihydrite: Evidence for the presence ofstructural hydroxyl groups. *Clay Miner.* **1979**, *14*, 109–114, doi:10.1180/claymin.1979.014.2.03.

26. Cornell, R. M.; Schwertmann, U. *The iron oxides: structure, properties, reactions, occurrences and uses*; John Wiley & Sons, 2003; ISBN 3527302743.

27. Vaughan, G.; Brydson, R.; Brown, A. Characterisation of Synthetic Two-line Ferrihydrite by Electron Energy Loss Spectroscopy. *J. Phys. Conf. Ser.* **2012**, *371*, 12079, doi:10.1088/1742-6596/371/1/012079.

28. Swedlund, P. J.; Miskelly, G. M.; McQuillan, A. J. Silicic acid adsorption and oligomerization at the ferrihydrite - Water interface: Interpretation of ATR-IR spectra based on a model surface structure. *Langmuir* **2010**, *26*, 3394–3401, doi:10.1021/la903160q.

29. Pokrovski, G. S.; Schott, J.; Farges, F.; Hazemann, J.-L. Iron (III)-silica interactions in aqueous solution: insights from X-ray absorption fine structure spectroscopy. *Geochim. Cosmochim. Acta* **2003**, *67*, 3559–3573, doi:10.1016/S0016-7037(03)00160-1.

30. Seehra, M. S.; Roy, P.; Raman, A.; Manivannan, A. Structural investigations of synthetic

ferrihydrite nanoparticles doped with Si. *Solid State Commun.* **2004**, *130*, 597–601, doi:10.1016/j.ssc.2004.03.022.

31. Dyer, L.; Fawell, P. D.; Newman, O. M. G.; Richmond, W. R. Synthesis and characterisation of ferrihydrite/silica co-precipitates. *J. Colloid Interface Sci.* **2010**, *348*, 65–70, doi:10.1016/j.jcis.2010.03.056.

32. Cismasu, A. C.; Michel, F. M.; Tcaciuc, A. P.; Brown, G. E. Properties of impurity-bearing ferrihydrite III. Effects of Si on the structure of 2-line ferrihydrite. *Geochim. Cosmochim. Acta* **2014**, *133*, 168–185, doi:10.1016/j.gca.2014.02.018.

33. Swedlund, P. J.; Miskelly, G. M.; McQuillan, A. J. An attenuated total reflectance IR study of silicic acid adsorbed onto a ferric oxyhydroxide surface. *Geochim. Cosmochim. Acta* **2009**, *73*, 4199–4214, doi:10.1016/j.gca.2009.04.007.

34. Hiemstra, T.; Barnett, M. O.; van Riemsdijk, W. H. Interaction of silicic acid with goethite. *J. Colloid Interface Sci.* **2007**, *310*, 8–17, doi:10.1016/j.jcis.2007.01.065.

35. Qi, P.; Pichler, T. Sequential and simultaneous adsorption of Sb(III) and Sb(V) on ferrihydrite: Implications for oxidation and competition. *Chemosphere* **2016**, *145*, 55–60, doi:10.1016/j.chemosphere.2015.11.057.

36. Leuz, A.; Mönch, H.; Johnson, C. A. Sorption of Sb (III) and Sb (V) to Goethite : Influence on Sb (III) Oxidation and Mobilization.

37. Stumm, W.; Morgan, J. J. *Aquatic chemistry: chemical equilibria and rates in natural waters*; John Wiley & Sons, 2012; Vol. 126;.

38. Wang, L.; Wan, C.; Zhang, Y.; Lee, D.-J.; Liu, X.; Chen, X.; Tay, J.-H. Mechanism of enhanced Sb(V) removal from aqueous solution using chemically modified aerobic granules. *J. Hazard. Mater.* **2015**, *284*, 43–49, doi:10.1016/j.jhazmat.2014.10.041.

39. Guo, X.; Wu, Z.; He, M. Removal of antimony(V) and antimony(III) from drinking water by coagulation-flocculation-sedimentation (CFS). *Water Res.* **2009**, *43*, 4327–4335, doi:10.1016/j.watres.2009.06.033.

40. Leuz, A.; Mo, H.; Johnson, C. A. Sorption of Sb (III) and Sb (V) to Goethite : Influence on Sb (III). **2006**, *40*, 7277–7282.

41. Jordan, N.; Marmier, N.; Lomenech, C.; Giffaut, E.; Ehrhardt, J. J. Competition between selenium (IV) and silicic acid on the hematite surface. *Chemosphere* **2009**, *75*, 129–134, doi:10.1016/j.chemosphere.2008.11.018.

42. Pokrovski, G. S.; Schott, J.; Farges, F.; Hazemann, J.-L. Iron (III)-silica interactions in aqueous solution: insights from X-ray absorption fine structure spectroscopy. *Geochim. Cosmochim. Acta* **2003**, *67*, 3559–3573.

461 43. Michel, F. M.; Ehm, L.; Antao, S. M.; Lee, P. L.; Chupas, P. J.; Liu, G.; Strongin, D. R.;
462 Schoonen, M. A. A.; Phillips, B. L.; Parise, J. B. The Structure of Ferrihydrite, a
463 Nanocrystalline Material. *Science (80-.).* **2007**, *316*, 1726–1729, doi:10.1126/science.1142525.